Applied Catalysis B: Environmental 325 (2023) 122369

Contents lists available at ScienceDirect

Applied Catalysis B: Environmental

journal homepage: www.elsevier.com/locate/apcatb

Boosting photocatalytic overall water splitting over single-layer graphene coated metal cocatalyst

Xinmin Yang [a], Jiwei Cui [a], Xiaolu Liu [a], Qiqi Zhang [a], Defa Wang [a], Jinhua Ye [a,b], Lequan Liu [a,*]

[a] TJU-NIMS International Collaboration Laboratory, Key Laboratory of Advanced Ceramics and Machining Technology (Ministry of Education), School of Materials Science and Engineering, Tianjin University, Tianjin 300072, P. R. China
[b] International Center for Materials Nanoarchitectonics (WPI-MANA), National Institute for Materials Science (NIMS), 1-1 Namiki, Tsukuba 305-0044, Japan

ARTICLE INFO

Keywords:
Graphene coating
Cocatalyst
Photocatalytic overall water splitting
Backward reaction
Chemical vapor deposition

ABSTRACT

Cocatalyst plays a critical role in photocatalytic overall water splitting (POWS). However, the typical metal cocatalysts aimed at promoting hydrogen evolution are also highly active for H_2-O_2 recombination. Here we report a new strategic approach of coating single-layer graphene selectively on metal cocatalyst by chemical vapor deposition to effectively suppress the backward reaction for efficient POWS. Pt@C/$SrTiO_3$ demonstrates steady POWS activity in contrast to the rapid activity decline by 65% in 5 h of Pt/$SrTiO_3$, and no obvious H_2 and O_2 consumption is observed over Pt@C/$SrTiO_3$ during dark reaction. Experimental and theoretical calculation results indicate that the graphene prevents O_2 from contacting Pt and the O_2 dissociation as the rate-determining step of backward reaction is retarded. Moreover, this method demonstrates good universality and similar suppressing effect is also achieved over Rh, Pd@C. These findings may open a new pathway for developing effective cocatalysts with suppressed backward reaction for efficient POWS.

1. Introduction

Photocatalytic overall water splitting (POWS) has been attracting much attention as an ideal way to generate clean and renewable hydrogen [1–4]. The major challenge is developing visible-light-response semiconductors and appropriate cocatalysts to make up efficient photocatalysts which are critical in promoting the efficiency of solar to hydrogen (STH) [5,6]. From the perspective of semiconductors, great advances have been achieved after tremendous efforts being made [7–11]. For example, $LaMg_xTa_{1-x}O_{1+3x}N_{2-3x}$ ($x > 1/3$) and $Y_2Ti_2O_5S_2$ with the theoretical STH reaching 16% and 20% respectively have been demonstrated to be promising photocatalyst materials [12,13]. Furthermore, two-step photo-excitation system named "Z-scheme" offers a helpful supplement to design POWS system based on the well-studied semiconductors in half-reaction [14–18]. As the other crucial component of photocatalyst for POWS, however, the achievement in cocatalyst is relatively limited [19].

Generally, metals (Pt, Rh, Pd, etc.) with large work functions are good candidates for hydrogen evolution reaction (HER) cocatalysts [20–22]. However, these metals are also highly active for the backward reaction between evolved H_2 and O_2 as well as maybe between atomic level intermediates like OH* at room temperatures, which largely restricts the efficiency of POWS [23–25]. In pursuit of suppressing the backward reaction, the core@shell structure has been demonstrated to be promising and effective [26–28], among which Rh@Cr_2O_3 is recognized as a typical and state-of-the-art example so far [29]. Nevertheless, the Cr_2O_3 shell strongly relies on the photodeposition method and can scarcely be prepared on semiconductors with a narrow bandgap [10,30]. Moreover, the Cr_2O_3 shell is prone to dissolve due to Cr^{3+} oxidation [31,32]. Hence, developing universal and effective cocatalysts for POWS is still highly desirable and of vital importance.

In constructing effective core@shell cocatalysts for POWS, the ideal shell material is expected to intercept O_2 and/or H_2 from the core metal nanoparticles (NPs) in addition to high conductivity to electrons. From this perspective, the graphene layer is attractive because the gap within its aromatic rings is blocked by the dense delocalized electron cloud of π-orbitals, which theoretically intercepts most molecules [33–36]. More importantly, Pt, Rh, Pd, etc. can solely serve as the active site in photocatalyst during coating graphene layer via catalytic graphitization [37–39]. Such an understanding inspires us to explore the effect of the graphene layer in suppressing the backward reaction for POWS which has not yet been reported.

Herein, we prepared core-shell structure of metal@C with graphene selectively coating on Pt, Rh, or Pd via chemical vapor deposition (CVD)

* Corresponding author.
E-mail address: Lequan.Liu@tju.edu.cn (L. Liu).

https://doi.org/10.1016/j.apcatb.2023.122369
Received 18 October 2022; Received in revised form 9 December 2022; Accepted 2 January 2023
Available online 4 January 2023

method, which demonstrated remarkably inhibited backward reaction for efficient POWS. The suppressing effect of graphene shell was revealed by experimental and theoretical studies that the graphene coating layer not only avoids Pt core from contacting O_2 but also remarkably retards the kinetics of water-formation backward reaction. Benefiting from this, the H_2 evolution rate of POWS over Pt@C/$SrTiO_3$/CoOOH was remarkably enhanced as compared with that of Pt/$SrTiO_3$/CoOOH.

2. Experimental section

2.1. Synthesis of $SrTiO_3$ (STO)

2 g of commercial $SrTiO_3$ and 20 g of $SrCl_2{\cdot}6\,H_2O$ were ground into a uniform powder. The powder was heated in an alumina crucible (100 mL) at 1373 K for 10 h in the air. After the furnace naturally cooled to room temperature, STO was washed with deionized (DI) water for 5 times and dried in the oven at 423 K for 5 h.

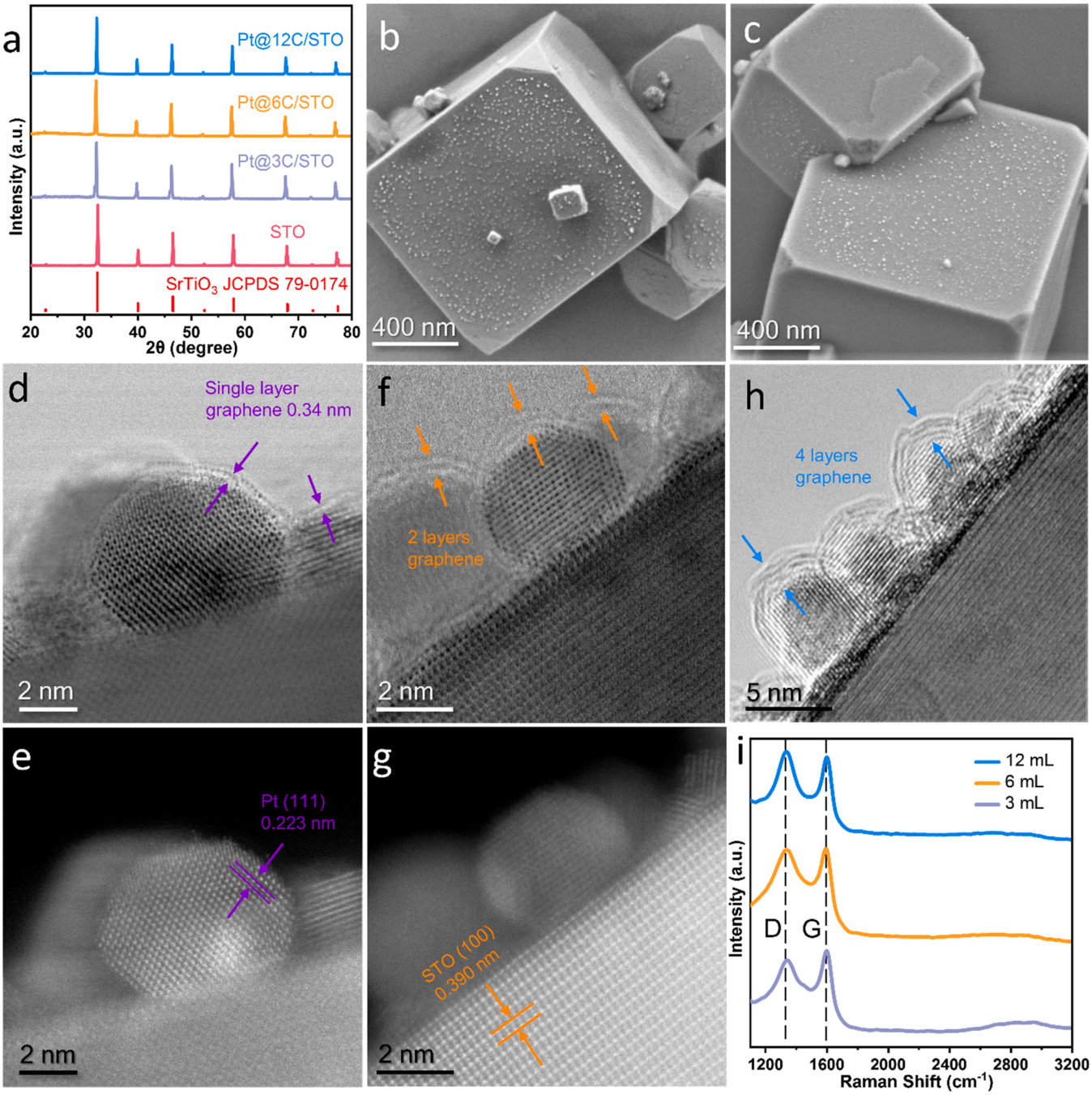

Fig. 1. Structure of Pt@C/STO. (a) XRD patterns of STO and Pt@C/STO. (b and c) SEM images of Pt/STO (b) and Pt@3C/STO (c). (d and e) ABF- and HAADF-STEM image of Pt@3C/STO. (f and g) ABF- and HAADF-STEM image of Pt@6C/STO. (h) HR-TEM image of Pt@12C/STO. (i) Raman spectra of Pt@xC/STO prepared with different volumes of C_2H_2.

2.2. Loading of metal cocatalyst on STO (M/STO)

The metal cocatalysts (0.25 wt%) were photodeposited on STO unless otherwise noted. The photodeposition of metal cocatalyst (Pt, Rh, Pd) was performed in the same reactor used in photocatalytic water splitting. 300 mg of STO and calculated amounts of precursors $H_6PtCl_6{\cdot}6\ H_2O$, $RhCl_3{\cdot}3\ H_2O$, or H_2PdCl_4 aqueous solution were dispersed in DI water (120 mL) with magnetic stirring. The suspension was completely degassed before being irradiated with a 300 W Xe lamp (full arc) for 1 h. M/STO was washed with deionized water for 3 times and dried in a vacuum drying oven at 333 K for 12 h. For the impregnation of Pt on STO (denote as Pt_{imp}/STO), 300 mg of STO and calculated amounts of $H_6PtCl_6{\cdot}6\ H_2O$ corresponding to 0.5 wt% Pt were dispersed in 5 mL of DI water and the mixture was heated on a water-bath at 353 K until dry. The powder was then calcined at 573 K for 1 h. Inductively Coupled Plasma (ICP) analysis of the impregnated sample indicated a final 0.3 wt% Pt depositing on STO.

2.3. Coating graphene selectively on metal deposited on STO (M@C/STO)

The metal NPs of M/STO was selectively coated by graphene layers through CVD method. The as-prepared M/STO was annealed at 873 K for 3 h under an atmosphere of Ar and H_2 (volume ratio of Ar: H_2 =9:1) mixed gas (100 sccm) in a vertical tubular furnace and the deposited metal species are reduced to metallic state. Then the gas was switched to Ar (100 sccm) with the temperature of the furnace maintained at 873 K for 2 h. 20 min after the reduction, C_2H_2 (3 sccm) was introduced into the tube for graphene growth. The layer number of graphene was tailored by varying the volume of C_2H_2 (carbon source), for example, 1 layer (3 mL), ~2 layers (6 mL), and ~4 layers (12 mL). Then the furnace cooled to room temperature naturally.

2.4. Synthesis of Rh@Cr_2O_3/STO/CoOOH

STO was modified with Rh@Cr_2O_3 and CoOOH through sequential photodeposition. Photodeposition was performed by dispersing 20 mg of STO in 120 mL of DI water in the same reactor used in photocatalytic water splitting. Calculated amounts of $RhCl_3{\cdot}3\ H_2O$ aqueous solution corresponding to 0.1 wt% Rh were added to the suspension. The suspension was completely degassed before being irradiated with a 300 W Xe lamp (full arc) for 10 min. Then K_2CrO_4 aqueous solution corresponding to 0.05 wt% Cr was added and irradiated for 5 min under vacuum. Subsequently, $Co(NO_3)_2{\cdot}3\ H_2O$ aqueous solution corresponding to 0.05 wt% Co was added and irradiated for another 5 min

2.5. Characterizations

The crystal structure of the samples was evaluated by an X − ray diffractometer (Bruker, Cu Kα radiation, D8 Advanced). The optical absorption spectra were characterized on an Ultraviolet-visible spectrophotometer (Shimadzu, UV-3600). The microstructure was observed by scanning transmission electron microscopy (STEM) (FEI-Titan Cubed Themis G2 300) and field-emission transmission electron microscopy (TEM) (JEOL, JEM-F200) and field-emission scanning electron microscopy (SEM) (FEI, Apreo S LoVac). Raman spectrum was obtained on a Raman microscope (HORIBA Scientific, Xplora PLUS). Time-resolved photoluminescence (PL) spectra were measured using a Fluorolog-3 (HORIBA Scientific) at 400 nm with 325 nm excitation. The chemical valence on the surface was analyzed by X − ray photoelectron spectroscopy (XPS) (Thermo Scientific, Escalab 250Xi), C 1s peak is corrected to 284.8 eV.

2.6. Photocatalytic water splitting

Photocatalytic water splitting was performed in a top-irradiated reactor connected to a closed gas circulation system. 20 mg of the photocatalyst was dispersed in 120 mL of DI water with magnetic stirring. The suspension was completely degassed before being irradiated with a 300 W Xe lamp (full arc). The evolved gases were analyzed by gas chromatograph (Shimadzu, GC−2014 with thermal conductivity detector, Ar carrier gas). The apparent quantum yield (AQY) for POWS involving one-step photoexcitation is calculated using: AQY(%)= [2 ×n(H_2)]/n(photons)× 100, where n(H_2) and n(photons) represent the number of produced H_2 molecules and incident photons, respectively. POWS were conducted using a 300 W Xe lamp with a water filter and a band-pass filter of 360 nm.

2.7. Electrochemical measurements

A three-electrode system was used for oxygen reduction reaction (ORR) and HER tests. An electrochemical workstation (CHI), an MSR electrode rotator (Pine), a saturated calomel electrode as the reference electrode, a glassy carbon rotating disk electrode (5 mm in diameter, 0.1963 cm^2 electrode surface area) as the working electrode and a graphite electrode as the counter electrode were used for all electrochemical measurements. The amount of Pt photodeposited on Pt/STO and Pt@C/STO that used in electrochemical tests is 5 wt% for the purpose of enhancing the conductivity of catalyst. The uniform suspension ink was prepared by dispersing 4 mg of catalyst into 420 μL of solution containing 200 μL of isopropanol, 200 μL of DI water and 20 μL of 5 wt% Nafion solution followed by 30 min of ultrasonication. 7 μL of ink was pipetted on the working electrode and dried at ambient temperature. Linear sweep voltammetry (LSV) measurements were recorded in O_2 or Ar saturated 0.5 M H_2SO_4 electrolyte solution for ORR (scan rate: 10 mV/s) and HER (scan rate: 20 mV/s), respectively. The rotating speed is 1600 rpm for HER and ranges from 400 to 1600 rpm for ORR.

3. Results and discussion

3.1. Structural characterization

To get broad insight into the principle of designing cocatalysts, $SrTiO_3$, one of the most well-known POWS photocatalysts, is employed as a model semiconductor. STO was prepared through flux method, and 0.25 wt% of Pt was photodeposited on STO (named Pt/STO). Different Pt@C/STO photocatalysts were fabricated through CVD process by controlling the volume of carbon source C_2H_2 (3, 6, and 12 mL), and the corresponding samples are denoted as Pt@xC/STO (x = 3, 6, and 12 respectively) (Fig. S1). The X-ray diffraction (XRD) patterns (Fig. 1a) of Pt@C/STO are indexed to $SrTiO_3$ phase (JCPDS card No. 79–0174), while no obvious peak of Pt or C is detected due to their low contents. SEM images of Pt/STO display the deposited Pt NPs are uniformly dispersed on the surface of cubic STO (Fig. 1b), and the CVD process makes little change to the morphology of either Pt or STO despite the amount of C_2H_2 (Fig. 1c and Fig. S2). The microstructure of Pt@C/STO is further studied by high-angle annular dark field (HAADF) and annular bright-field (ABF) STEM (Fig. 1d-g). Pt NPs with average diameters of about 4–5 nm (Fig. S3) are found homogeneously dispersed on STO, and the lattice spacing of 0.223 nm corresponds to the (111) plane of Pt (Fig. 1e). For Pt@3C/STO, ABF-STEM and high resolution (HR) TEM images demonstrate that single layer of graphene with the thickness of 0.34 nm is coated on Pt (Fig. 1d and Fig. S4) [33]. Along with the amount of C_2H_2 increasing to 6 and 12 mL, the coating graphene rise to ~2 and ~4 layers respectively (Fig. 1f, h; Figs. S5 and S6). It is worth pointing out the graphene is selectively coated on Pt rather than STO due to the sole activity of Pt NPs for catalyzing graphitization. Benefitting from this, there is no significant change in the optical properties between Pt@C/STO and STO (Fig. S7), which insures the light absorption of semiconductor. Moreover, the high graphitization of graphene is demonstrated by the characteristic G band at 1605 cm^{-1} in Raman spectra (Fig. 1i and Fig. S8) [40,41]. The D peak should mainly originate

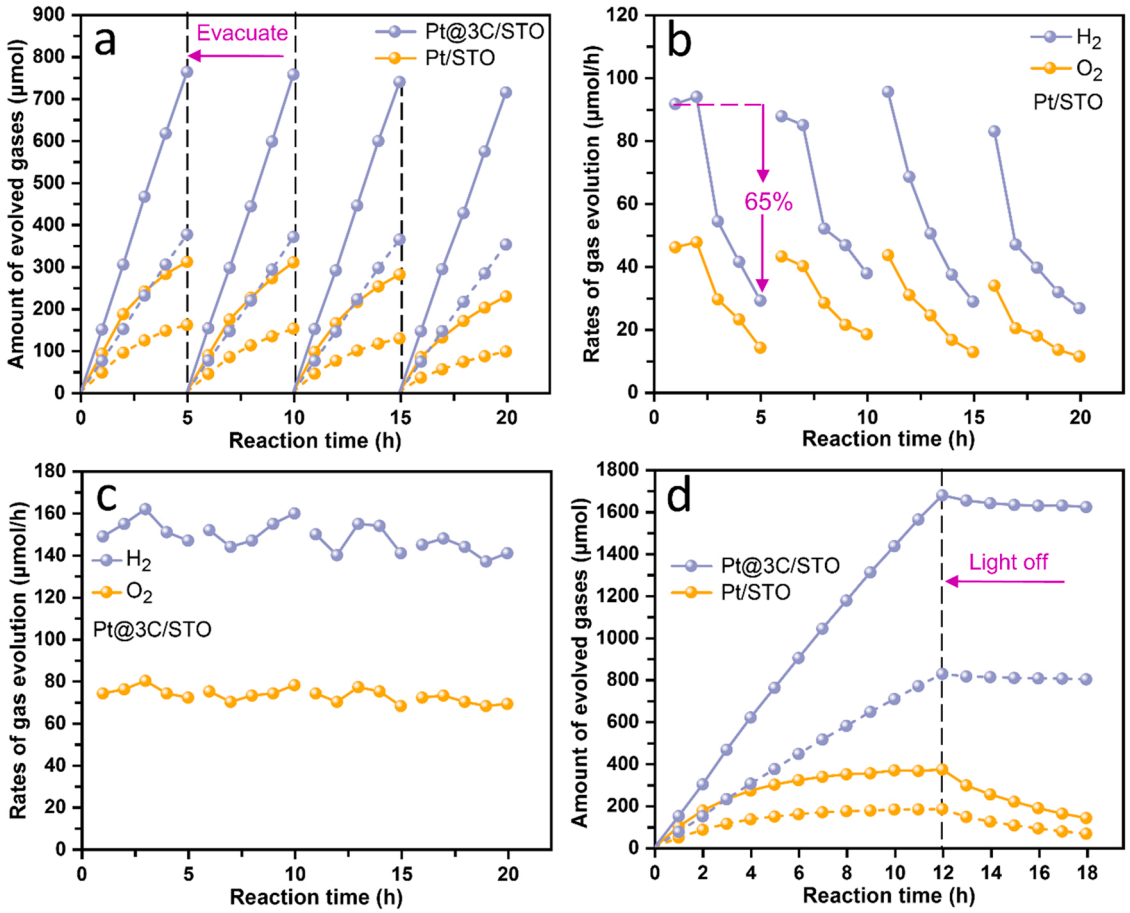

Fig. 2. Backward reaction suppression in photocatalytic overall water splitting test. (a) Time course of POWS on Pt/STO and Pt@3C/STO for 20 h, with evacuation every 5 h, solid and dashed line represents H_2 and O_2, respectively. (b and c) Rates of gas evolution during 20 h POWS tests for Pt/STO (b) and Pt@3C/STO (c). (d) Time course of POWS under irradiation for 12 h and dark reaction for 6 h on Pt/STO and Pt@3C/STO, solid and dashed line represents H_2 and O_2, respectively. Reaction condition: photocatalyst (20 mg) loaded with Pt (0.25 wt%); DI water (120 mL); light
Source: 300 W Xe lamp.

from small domain size of graphene, the abundance of edges of nano-graphene coating [42–44], and non-perfect honeycomb lattice structure of spherical graphene coatings [35].

3.2. *Suppression of backward reaction over Pt@C cocatalyst for efficient POWS*

We performed POWS over Pt/STO and Pt@3C/STO for 4 continuous runs with the gases evacuated after every cycle (Fig. 2a) under the illumination of a 300 W Xe lamp; the average light intensity is 1060 mW/cm^2 (Fig. S9 and Table S1). The molar ratios of evolved H_2 and O_2 were close to the stoichiometric value of 2:1, suggesting POWS was underway. For Pt/STO, the initial H_2 evolution rate was 92 μmol h^{-1}, which basically agrees with early reports [45,46]. However, it dropped rapidly by 65% to 30 μmol h^{-1} at the 5th hour (Fig. 2b). Notably, after every evacuation and re-running the experiment, the gas evolution rates almost returned to the initial values of the first run. These results suggest that it is more likely the deceleration of gases evolution should be mainly caused by H_2-O_2 backward reaction on naked Pt [47–49]. By contrast, the H_2 evolution rate of 149 μmol h^{-1} was achieved over Pt@3C/STO (Fig. 2c), and the amount of the evolved gases for Pt@3C/STO was in a good linear relationship to the reaction time even though the accumulated amount at the end of every cycle is ~2.5 times as many as that of Pt/STO, i.e., the gases evolution rate maintained well. The annealing process during the CVD shows no obvious influence on the performance of STO and Pt/STO (Fig. S10). These results indicate the backward reaction are remarkably suppressed and maybe even at atomic level [24]. Similar steady gas evolutions are also observed for Pt@6C/STO and Pt@12C/STO with the rate of H_2 evolution at ~100 and ~61 μmol h^{-1} in POWS respectively (Figs. S11 and S12). The inferior activity of Pt@6C/STO and Pt@12C/STO may be because the transfer of electrons decays with increasing layers of graphene [50–52].

The suppressing effect of graphene was further clarified by prolonged irradiation experiment (Fig. 2d). For Pt/STO, the gases evolution rate continuously declined to nearly zero at the 8th hour and the reaction reached a plateau. Impressively, for Pt@3C/STO, the gas evolution rates maintained well in 12 h. The light was then turned off for dark reaction. For Pt/STO, the stored H_2 and O_2 decreased with initial rates of 75 and 37 μmol h^{-1} respectively. This H_2-O_2 consumption ratio of ca. 2:1 confirms the thermocatalytic H_2-O_2 backward reaction proceeds obviously at the operation temperature, so the plateau of reaction during irradiation corresponds to the equilibration between forward reaction and backward reaction [47,53]. In contrast, for Pt@3C/STO, no obvious gas consumption was observed although the accumulated gases are 4.5 times as many as that of Pt/STO. The characterizations of Raman spectroscopy, XPS, and TEM indicated that Pt@3C/STO did not undergo obvious change after POWS for 12 h (Fig. S13). Moreover, we also investigated the effectiveness of graphene coating by changing the loading method of metal NPs and using other semiconductor. As can be seen, similar effect of graphene coating in suppressing backward reaction was achieved on Pt_{imp}@C/STO (Fig. S14) and Pt@C/$NaTaO_3$:La

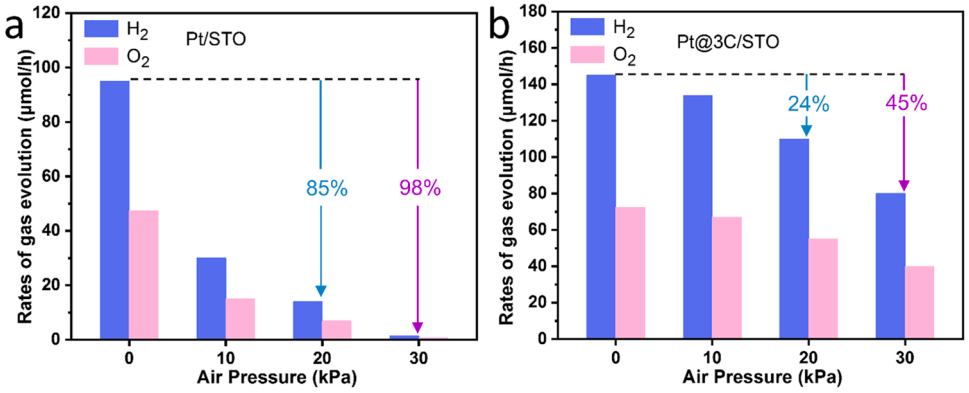

Fig. 3. Effect of initial background pressure of air on POWS rate. Dependence of gas evolution rates on (a) Pt/STO, and (b) Pt@3C/STO upon the initial background pressure of air in the reaction system. Reaction condition: photocatalyst (20 mg) loaded with Pt (0.25 wt%); DI water (120 mL); light Source: 300 W Xe lamp.

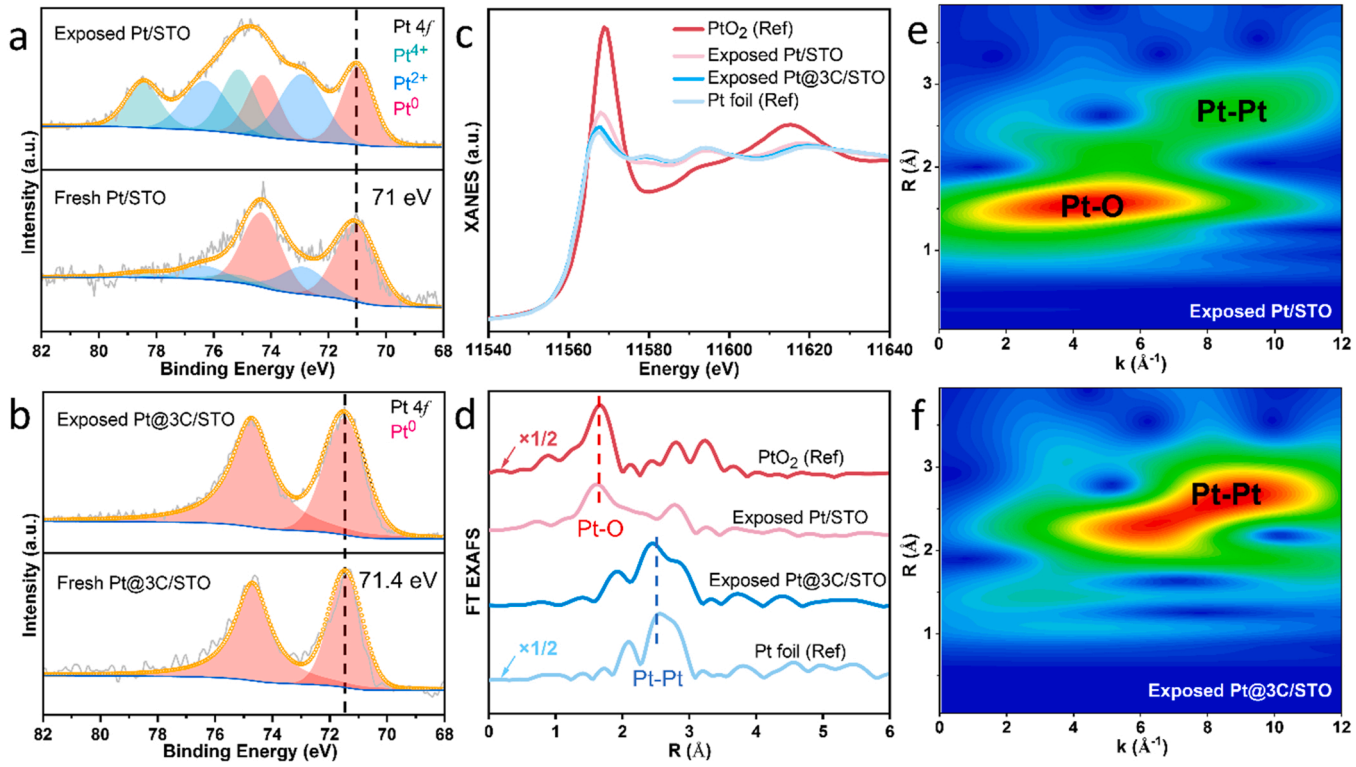

Fig. 4. XPS and XAS characterizations. (a and b) XPS Pt 4f spectra of Pt/STO (a) and Pt@3C/STO (b) before and after exposing experiment. (c and d) Pt L_3-edge XANES spectra and the k^2-weighted Fourier transform EXAFS spectra of exposed Pt/STO and exposed Pt/STO, as well as Pt foil and PtO_2 references. (e and f) Contour plot of wavelet transform magnitude of exposed Pt/STO (e) and exposed Pt@3C/STO (f).

(Fig. S15). These results suggest the good universality of our strategic approach in preparing effective Pt@C cocatalyst, which breaks through the requirement on the wide bandgap of semiconductor in contrast to the photodeposition of Cr_2O_3 on metal NPs.

3.3. Influence of the elevated background pressure of air on POWS activity

The attractive goal of POWS is H_2 evolution at ambient conditions including air atmosphere. Fig. 3 shows the evaluation of POWS rate upon the background air introduced into the reaction system before irradiation. For Pt/STO, the gas evolution rates drop drastically upon raising the amount of air, and 30 kPa background pressure leads to a decline of 98%. Though the decrease in evolution rate can be expected due to elevated operation pressure, a nearly total loss of POWS activity is notable, which should be closely related to the backward reaction and partial passivation of Pt after exposure to air. By contrast, Pt@3C/STO retained 76% and 55% of its original performance at the air background pressure of 20 and 30 kPa respectively, and one-third of POWS activity was maintained even at 70 kPa of air (Fig. S16). That is, Pt@C demonstrates high stability and resistance to air, which is very helpful for the practical application of POWS.

3.4. Backward reaction suppression mechanism over Pt@C

To get insight into the mechanism of backward reaction suppression on Pt@C, the possibility of H_2-O_2 recombining on the surface of both Pt core and graphene shell were investigated respectively. For the former,

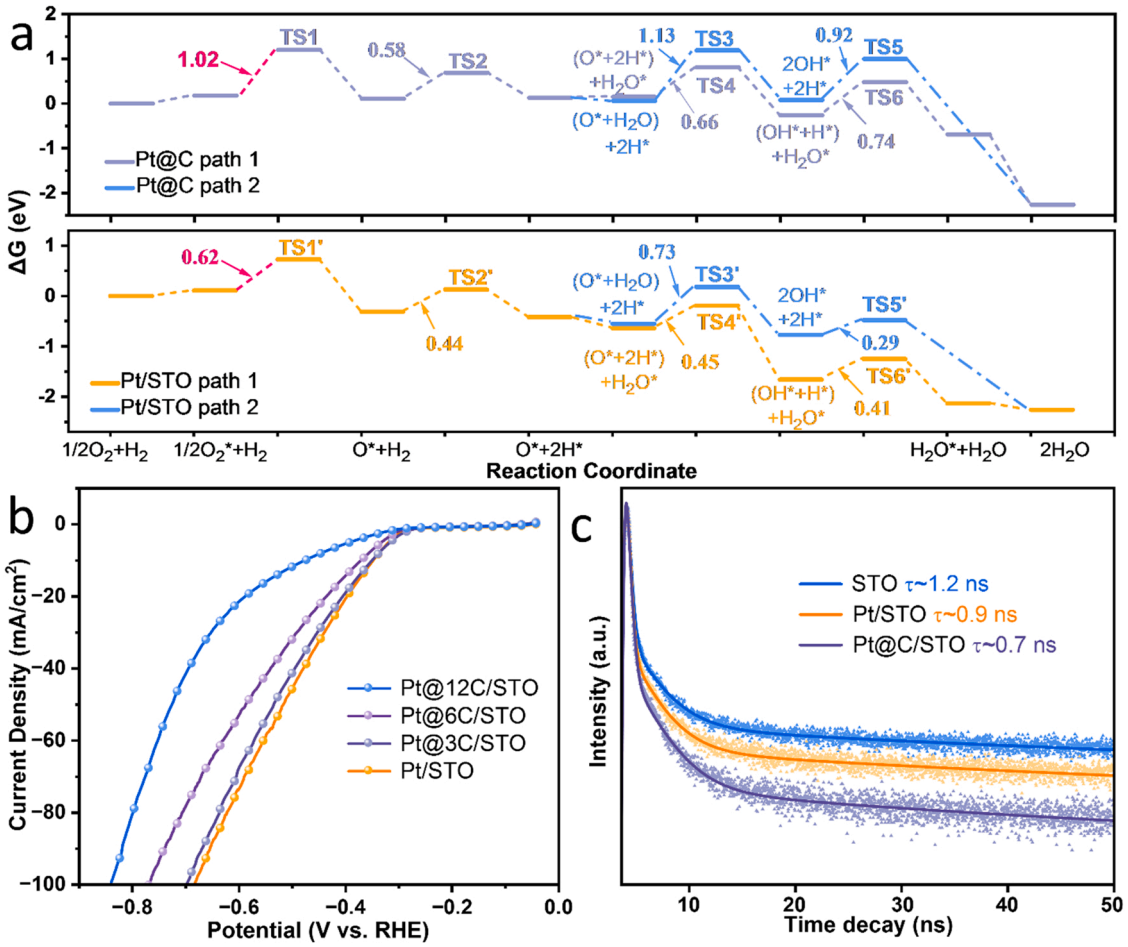

Fig. 5. Study of surface reaction and PL lifetime. (a) Potential energy diagram for the water formation from H_2 reacting with O_2 on Pt_{130}/STO and $Pt_{130}@C_{161}$/STO. (b) HER LSV curves of Pt/STO and Pt@C/STO, performed in Ar-saturated 0.5 M aqueous H_2SO_4 solution. (c) Time-resolved PL decay spectra of various photocatalysts.

whether O_2 can reach the surface of Pt coated by graphene was studied by X-ray absorption spectroscopy (XAS) and XPS by probing the chemical state of samples exposed to ambient air. The XPS spectra of Pt 4f display mildly oxidized Pt for fresh Pt/STO and sole Pt^0 for fresh Pt@3C/STO (Fig. 4a, b) [54]. For exposed Pt/STO, the X-ray absorption near-edge structure (XANES) spectra in Fig. 4c show the white-line intensity of Pt L_3-edge is higher than Pt foil, demonstrating the chemical state of Pt on exposed Pt/STO is positive. The coordination of Pt is further revealed by extended X-ray absorption fine structure (EXAFS) investigation (Fig. 4d and Table S2). Exposed Pt/STO exhibits a main peak at about 1.6 Å ascribed to Pt-O coordination, which is in agreement with the wavelet transform (WT) analysis of the intensity maximum at about (4.5 $Å^{-1}$, 1.6 Å) being ascribed to Pt-O coordination (Fig. 4e and Fig. S17). In contrast, Pt NPs on exposed Pt@3C/STO are demonstrated to be metallic by the same white-line intensity as Pt foil and the sole Pt-Pt coordination at 2.6 Å (Fig. 4c, f). XPS results indicate the Pt of Pt@3C/STO remain metallic even after exposure for 3 months while most of the surface Pt on exposed-Pt/STO are oxidized to be $Pt^{2+/4+}$ (Fig. 4a, b). The Pt^0 4f peaks of Pt@3C/STO shifting to a higher energy than that of Pt/STO demonstrates the strong electron transfer from Pt NPs to graphene with good conductivity to electron [40,55,56]. Taken together, unlike the oxidation of Pt on exposed Pt/STO, Pt NPs of exposed Pt@3C/STO maintaining metallic well clarify that graphene coating prevents Pt from contacting O_2, which rules out the possibility of direct water-formation backward reaction on the surface of Pt core.

We further study the H_2-O_2 backward reaction on graphene shell of Pt@C by density functional theory (DFT) calculations. Two catalyst models of Pt covered by single-layer graphene ($Pt_{130}@C_{161}$) and naked Pt_{130} supported on STO (Fig. S18) were constructed on account of STEM results (Fig. 1f). The elemental steps of $H_2 + 1/2\ O_2 \rightarrow H_2O$ commonly include (i) adsorption and dissociation of H_2 and O_2 and (ii) formation of intermediate OH* through the pathway of $O^* + H^* \rightarrow OH^* + *$ or $O^* + H_2O^* \rightarrow 2OH^*$ and (iii) the addition of H* to OH* to form H_2O [57,58]. Fig. 5a shows the comparison of the formation of intermediate OH* - through path1 of $O^* + H^* \rightarrow OH^* + *$ and path2 of $O^* + H_2O^* \rightarrow 2OH^*$. For step two, the calculations on both $Pt_{130}@C_{161}$/STO and Pt_{130}/STO indicate the direct coupling of H* and O* (i.e., path1) is dynamically preferential (Figs. S19 and S20). Thus the detailed pathways of H_2-O_2 backward reaction were determined and the potential energy diagram was plotted. It is clear that the barrier of every step on $Pt_{130}@C_{161}$/STO is higher as compared with Pt_{130}/STO. Especially for the rate-determining step of O_2 dissociation, the barrier of $Pt_{130}@C_{161}$/STO is 1.6 times as high as that of Pt_{130}/STO (0.62 eV). These results indicate the H_2-O_2 recombination on $Pt_{130}@C_{161}$/STO is remarkably hampered because of the retarded kinetics. Meanwhile, the higher dissociative absorption barrier of O_2 also suggests that the ORR on the outer surface of graphene coating on Pt is much more difficult than that on the surface of Pt, which agrees well with the electrochemical ORR studies (Fig. S21) [59]. The limiting diffusion current of Pt/STO is much larger than that of Pt@C/STO. Besides, in contrast to Pt/STO exhibiting typical rotation-dependent Levich behavior, there is no change in the ORR on Pt@C/STO when improving the mass transport of the dissolved oxygen by increasing the rotation speed, demonstrating the ORR on Pt@C/STO is hindered by monolayer graphene coating [45,60].

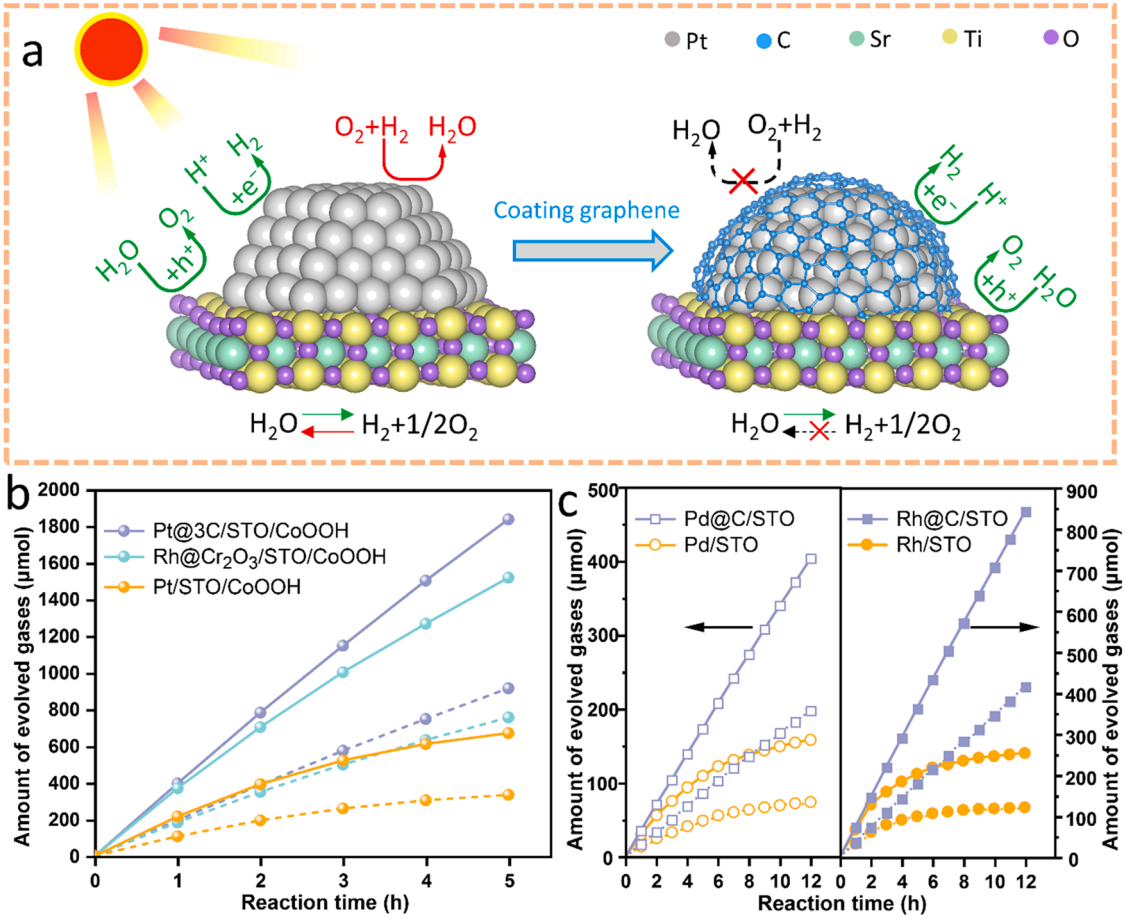

Fig. 6. Effectiveness and universality of graphene coating strategy. (a) Schematic diagram for POWS reaction over Pt/STO and Pt@C/STO. (b) Time course of POWS on Pt@3C/STO/CoOOH (0.1 wt% Pt, 0.05 wt% Co), Rh@Cr_2O_3/STO/CoOOH (0.1 wt% Rh, 0.05 wt% Cr, 0.05 wt% Co) and Pt/STO/CoOOH (0.1 wt% Pt, 0.05 wt% Co). (c) Time course of POWS on Pd@C/STO (0.25 wt% Pd) and Rh@C/STO (0.25 wt% Rh). Solid and dashed line represents H_2 and O_2, respectively. Reaction condition: photocatalyst (20 mg); DI water (120 mL); light
Source: 300 W Xe lamp.

Though similar suppressing effect is observed, these results indicate that the mechanism for Pt@C is different from the typical cocatalysts for POWS like Rh@Cr_2O_3 which are constructed by coating noble metal NPs with amorphous metal oxyhydroxide hydrate. Previous studies have demonstrated that the metal oxyhydroxide hydrate layer is penetrable for both H_2 and O_2, while the reverse reaction is suppressed by the unfavourable O_2 penetrating due to relatively low background pressure [30,45,61]. However, the above results together with XPS and XAS characterizations reveal that the graphene coating for Pt@C effectively blocks off O_2 from contacting Pt even under ambient pressure and retards the kinetics of H_2 oxidation with O_2 on the surface of Pt@C, which is beneficial and attractive for the potential application of POWS operated under ambient conditions. Furthermore, LSV measurements for electrochemical HER in Fig. 5b verify that the HER activity of Pt is not notably influenced by the monolayer graphene coating, which is also supported by the effective transfer of electrons from Pt NPs to graphene (Fig. 4a, b) and the adsorption free energy of H (ΔG_{H^*}) (Fig. S22) [62–65]. Moreover, the behavior of photoexcited charge transfer and recombination were investigated by time-resolved PL. As shown in Fig. 5c, the fluorescence lifetime of Pt/STO and Pt@C/STO is about 25% and 42% shorter than that of STO, respectively, indicating graphene coating layer can also suppress photoexcited electron-hole recombination. This may result from the enhancement of graphene coating for the interfacial separation and transfer of photoexcited carriers, which should be beneficial to the activity of POWS [66–68].

3.5. *Effectiveness and universality of coating graphene on metal NPs for suppressing backward reaction*

Fig. 6a illustrates the photocatalytic overall water splitting and reverse reaction processes over Pt/STO and Pt@C/STO. Both Pt NPs and Pt@C cocatalysts can act as H_2 evolution site on STO surface, whereas the undesirable H_2-O_2 reverse reaction is facilitated by Pt NPs. After selectively coating graphene on Pt NPs, the graphene coating not only blocks off O_2 from contacting Pt but also retarding the kinetics of H_2 oxidation with O_2 on the surface of Pt@C, therefore, the H_2-O_2 reverse reaction is effectively inhibited over Pt@C. For comprehensively evaluating the POWS performance, CoOOH is further photodeposited as oxygen evolution reaction cocatalyst. As can be seen from Fig. 6b, steady gas evolution rates of ~396 μmol h^{-1} (H_2) and ~196 μmol h^{-1} (O_2) were achieved over Pt@3C/STO/CoOOH, which is superior to Rh@Cr_2O_3/STO/CoOOH. Remarkably, the demonstrated rates were 2.7 times as high as that of Pt/$SrTiO_3$/CoOOH. The AQY of Pt@3C/STO/CoOOH is 44.0%@360 nm and the comparison with other photocatalysts are listed in Table S3 and S4. Considering the superior effect of Pt@C on $SrTiO_3$-flux and the notably promoted intrinsic activity of $SrTiO_3$ by doping, it can be reasonably expected that a more competitive POWS efficiency can definitely be obtained by adopting more efficient $SrTiO_3$ [2,29,69]. Moreover, overall water splitting was tested in ambient conditions over a Pt@3C/STO/CoOOH photocatalyst sheet (5 ×5 cm^2 loaded with 20 mg of catalyst) and a video was recorded for intuitive observation of the performance (see Supporting information). Besides, Pd@C and

Rh@C were also successfully prepared by a similar procedure as Pt@C (Fig. S23). Steady H_2 and O_2 evolution were achieved over Pd@C/STO and Rh@C/STO, which is in sharp contrast to the gradually suppressed gases evolution over Pd/STO and Rh/STO owing to the backward reaction (Fig. 6c). These results demonstrate the effectiveness and universality of this strategic approach to suppressing the backward reaction through selectively coating graphene on metal cocatalysts for efficient POWS.

4. Conclusion

In conclusion, metal@C prepared by selectively coating graphene on metal NPs (Pt, Rh, or Pd) has been demonstrated to be highly efficient cocatalysts for POWS. Compared with its counterpart, the backward reaction is significantly suppressed over Pt@C, which enables efficient and steady gas evolution in POWS. Experimental and theoretical studies revealed that the graphene coating plays a key role in suppressing backward reaction. XAS and XPS studies provide clear evidence that graphene coating prevents Pt core from directly contacting O_2, and DFT calculations further indicate that the graphene coating on Pt greatly obstructs the rate-determining O_2 dissociation, thus the backward reaction on the surface of both Pt and graphene coating are both suppressed. Moreover, Pt@3C/STO/CoOOH achieved POWS with a steady H_2 evolution rate of ~396 μmol h^{-1}, which is superior to the typical Rh@Cr_2O_3/STO/CoOOH. Such a facile and effective strategy of selectively coating graphene on metal NPs for metal@C cocatalysts is expected to be helpful in suppressing backward reaction for better boosting photocatalytic overall water splitting.

CRediT authorship contribution statement

Xinmin Yang: Conceptualization, Investigation, Writing – original draft. **Jiwei Cui:** Investigation, Software. **Xiaolu Liu:** Investigation. **Qiqi Zhang:** Investigation. **Defa Wang:** Resources. **Jinhua Ye:** Resources, Writing – review & editing. **Lequan Liu:** Funding acquisition, Supervision, Conceptualization, Writing – review & editing.

Declaration of Competing Interest

The authors declare that they have no known competing financial interests or personal relationships that could have appeared to influence the work reported in this paper.

Data Availability

Data will be made available on request.

Acknowledgments

We acknowledge support from the National Natural Science Foundation of China (22072106) and National Key Research and Development Program of China (2021YFA1500800).

Supplementary material

Supporting Information Available: UV–vis absorption spectra, SEM, TEM, photocatalytic measurements, Raman spectra, XPS, and DFT calculations (PDF). Video depicting the evolution of oxyhydrogen bubbles on a Pt@3C/STO/CoOOH photocatalyst sheet under a 300 W Xe lamp in ambient conditions (MP4).

Appendix A. Supporting information

Supplementary data associated with this article can be found in the online version at doi:10.1016/j.apcatb.2023.122369.

References

[1] A. Fujishima, K. Honda, Electrochemical photolysis of water at a semiconductor electrode, Nature 238 (1972) 37–38, https://doi.org/10.1038/238037a0.
[2] H. Nishiyama, T. Yamada, M. Nakabayashi, Y. Maehara, M. Yamaguchi, Y. Kuromiya, H. Tokudome, S. Akiyama, T. Watanabe, R. Narushima, S. Okunaka, N. Shibata, T. Takata, T. Hisatomi, K. Domen, Photocatalytic solar hydrogen production from water on a 100 m^2-scale, Nature 598 (2021) 304–307, https://doi.org/10.1038/s41586-021-03907-3.
[3] H. Tong, S. Ouyang, Y. Bi, N. Umezawa, M. Oshikiri, J. Ye, Nano-photocatalytic materials: possibilities and challenges, Adv. Mater. 24 (2012) 229–251, https://doi.org/10.1002/adma.201102752.
[4] R. Chen, Z. Ren, Y. Liang, G. Zhang, T. Dittrich, R. Liu, Y. Liu, Y. Zhao, S. Pang, H. An, C. Ni, P. Zhou, K. Han, F. Fan, C. Li, Spatiotemporal imaging of charge transfer in photocatalyst particles, Nature 610 (2022) 296–301, https://doi.org/10.1038/s41586-022-05183-1.
[5] Q. Wang, K. Domen, Particulate photocatalysts for light-driven water splitting: mechanisms, challenges, and design strategies, Chem. Rev. 120 (2020) 919–985, https://doi.org/10.1021/acs.chemrev.9b00201.
[6] X. Li, Y. Chen, Y. Tao, L. Shen, Z. Xu, Z. Bian, H. Li, Challenges of photocatalysis and their coping strategies, Chem. Catal. 2 (2022) 1315–1345, https://doi.org/10.1016/j.checat.2022.04.007.
[7] S. Chen, T. Takata, K. Domen, Particulate photocatalysts for overall water splitting, Nat. Rev. Mater. 2 (2017) 17050, https://doi.org/10.1038/natrevmats.2017.50.
[8] Z.G. Zou, J.H. Ye, K. Sayama, H. Arakawa, Direct splitting of water under visible light irradiation with an oxide semiconductor photocatalyst, Nature 414 (2001) 625–627, https://doi.org/10.1038/414625a.
[9] K. Maeda, T. Takata, M. Hara, N. Saito, Y. Inoue, H. Kobayashi, K. Domen, GaN: ZnO solid solution as a photocatalyst for visible-light-driven overall water splitting, J. Am. Chem. Soc. 127 (2005) 8286–8287, https://doi.org/10.1021/ja0518777.
[10] Z. Wang, Y. Inoue, T. Hisatomi, R. Ishikawa, Q. Wang, T. Takata, S. Chen, N. Shibata, Y. Ikuhara, K. Domen, Overall water splitting by Ta_3N_5 nanorod single crystals grown on the edges of $KTaO_3$ particles, Nat. Catal. 1 (2018) 756–763, https://doi.org/10.1038/s41929-018-0134-1.
[11] Z. Bian, J. Zhu, H. Li, Solvothermal alcoholysis synthesis of hierarchical TiO_2 with enhanced activity in environmental and energy photocatalysis, J. Photochem. Photobiol. C. 28 (2016) 72–86, https://doi.org/10.1016/j.jphotochemrev.2016.06.002.
[12] Q. Wang, M. Nakabayashi, T. Hisatomi, S. Sun, S. Akiyama, Z. Wang, Z. Pan, X. Xiao, T. Watanabe, T. Yamada, N. Shibata, T. Takata, K. Domen, Oxysulfide photocatalyst for visible-light-driven overall water splitting, Nat. Mater. 18 (2019) 827–832, https://doi.org/10.1038/s41563-019-0399-z.
[13] C. Pan, T. Takata, M. Nakabayashi, T. Matsumoto, N. Shibata, Y. Ikuhara, K. Domen, A complex perovskite-type oxynitride: the first photocatalyst for water splitting operable at up to 600 nm, Angew. Chem. Int. Ed. 54 (2015) 2955–2959, https://doi.org/10.1002/anie.201410961.
[14] J. Abdul Nasir, A. Munir, N. Ahmad, Tu Haq, Z. Khan, Z. Rehman, Photocatalytic Z-scheme overall water splitting: recent advances in theory and experiments, Adv. Mater. 33 (2021) 2105195, https://doi.org/10.1002/adma.202105195.
[15] Y. Qi, J. Zhang, Y. Kong, Y. Zhao, S. Chen, D. Li, W. Liu, Y. Chen, T. Xie, J. Cui, C. Li, K. Domen, F. Zhang, Unraveling of cocatalysts photodeposited selectively on facets of $BiVO_4$ to boost solar water splitting, Nat. Commun. 13 (2022) 484–492, https://doi.org/10.1038/s41467-022-28146-6.
[16] Q. Wang, T. Hisatomi, Y. Suzuk, Z. Pan, J. Seo, M. Katayama, T. Minegishi, H. Nishiyama, T. Takata, K. Seki, A. Kudo, T. Yamada, K. Domen, Particulate photocatalyst sheets based on carbon conductor layer for efficient Z-scheme pure-water splitting at ambient pressure, J. Am. Chem. Soc. 139 (2017) 1675–1683, https://doi.org/10.1021/jacs.6b12164.
[17] D. Zhao, Y. Wang, C.-L. Dong, Y.-C. Huang, J. Chen, F. Xue, S. Shen, L. Guo, Boron-doped nitrogen-deficient carbon nitride-based Z-scheme heterostructures for photocatalytic overall water splitting, Nat. Energy 6 (2021) 388–397, https://doi.org/10.1038/s41560-021-00795-9.
[18] Q. Zhang, M. Liu, W. Zhou, Y. Zhang, W. Hao, Y. Kuang, H. Liu, D. Wang, L. Liu, J. Ye, A novel Cl^- modification approach to develop highly efficient photocatalytic oxygen evolution over BiVO4 with AQE of 34.6%, Nano Energy 81 (2021), 105651 https://doi.org/10.1016/j.nanoen.2020.105651.
[19] B. Mei, K. Han, G. Mul, Driving surface redox reactions in heterogeneous photocatalysis: the active state of illuminated semiconductor-supported nanoparticles during overall water-splitting, ACS Catal. 8 (2018) 9154–9164, https://doi.org/10.1021/acscatal.8b02215.
[20] X. Zong, H. Yan, G. Wu, G. Ma, F. Wen, L. Wang, C. Li, Enhancement of photocatalytic H_2 evolution on CdS by loading MoS_2 as cocatalyst under visible light irradiation, J. Am. Chem. Soc. 130 (2008) 7176–7177, https://doi.org/10.1021/ja8007825.
[21] M. Wang, W.L. Zhen, B. Tian, J.T. Ma, G.X. Lu, The inhibition of hydrogen and oxygen recombination reaction by halogen atoms on over-all water splitting over Pt-TiO_2 photocatalyst, Appl. Catal. B Environ. 236 (2018) 240–252, https://doi.org/10.1016/j.apcatb.2018.05.031.
[22] X. Chen, J. Wang, Y. Chai, Z. Zhang, Y. Zhu, Efficient photocatalytic overall water splitting induced by the giant internal electric field of a g-C_3N_4/rGO/PDIP Z-scheme heterojunction, Adv. Mater. 33 (2021) 2007479, https://doi.org/10.1002/adma.202007479.
[23] B. Qiu, M. Du, Y. Ma, Q. Zhu, M. Xing, J. Zhang, Integration of redox cocatalysts for artificial photosynthesis, Energy Environ. Sci. 14 (2021) 5260–5288, https://doi.org/10.1039/D1EE02359D.

[24] D.C. Skelton, R.G. Tobin, G.B. Fisher, D.K. Lambert, C.L. DiMaggio, Suppression of water formation over stepped Pt(335) by Au, J. Phys. Chem. B 104 (2000) 548–553, https://doi.org/10.1021/jp9916211.

[25] W. Gao, B. Tian, W.Y. Zhang, X.Q. Zhang, Y.Q. Wu, G.X. Lu, NIR light driven catalytic hydrogen generation over semiconductor photocatalyst coupling up-conversion component, Appl. Catal. B Environ. 257 (2019) 9, https://doi.org/10.1016/j.apcatb.2019.117908.

[26] M. Yoshida, K. Maeda, D. Lu, J. Kubota, K. Domen, Lanthanoid oxide layers on rhodium-loaded $(Ga_{1-x}Zn_x)(N_{1-x}O_x)$ photocatalyst as a modifier for overall water splitting under visible-light irradiation, J. Phys. Chem. C 117 (2013) 14000–14006, https://doi.org/10.1021/jp402240d.

[27] T.F. Berto, K.E. Sanwald, J.P. Byers, N.D. Browning, O.Y. Gutiérrez, J.A. Lercher, Enabling overall water splitting on photocatalysts by CO-covered noble metal co-catalysts, J. Phys. Chem. Lett. 7 (2016) 4358–4362, https://doi.org/10.1021/acs.jpclett.6b02151.

[28] Z. Zeng, X. Quan, H. Yu, S. Chen, W. Choi, B. Kim, S. Zhang, Alkali-metal-oxides coated ultrasmall Pt sub-nanoparticles loading on intercalated carbon nitride: Enhanced charge interlayer transportation and suppressed backwark reaction for overall water splitting, J. Catal. 377 (2019) 72–80, https://doi.org/10.1016/j.jcat.2019.07.018.

[29] T. Takata, J. Jiang, Y. Sakata, M. Nakabayashi, N. Shibata, V. Nandal, K. Seki, T. Hisatomi, K. Domen, Photocatalytic water splitting with a quantum efficiency of almost unity, Nature 581 (2020) 411–414, https://doi.org/10.1038/s41586-020-2278-9.

[30] T. Takata, C. Pan, M. Nakabayashi, N. Shibata, K. Domen, Fabrication of a core–shell-type photocatalyst via photodeposition of group IV and V transition metal oxyhydroxides: an effective surface modification method for overall water splitting, J. Am. Chem. Soc. 137 (2015) 9627–9634, https://doi.org/10.1021/jacs.5b04107.

[31] Q. Wang, S. Okunaka, H. Tokudome, T. Hisatomi, M. Nakabayashi, N. Shibata, T. Yamada, K. Domen, Printable photocatalyst sheets incorporating a transparent conductive mediator for Z-scheme water splitting, Joule 2 (2018) 2667–2680, https://doi.org/10.1016/j.joule.2018.08.003.

[32] T. Nishino, M. Saruyama, Z. Li, Y. Nagatsuma, M. Nakabayashi, N. Shibata, T. Yamada, R. Takahata, S. Yamazoe, T. Hisatomi, K. Domen, T. Teranishi, Self-activated Rh-Zr mixed oxide as a nonhazardous cocatalyst for photocatalytic hydrogen evolution, Chem. Sci. 11 (2020) 6862–6867, https://doi.org/10.1039/d0sc01363c.

[33] X. Li, W. Cai, J. An, S. Kim, J. Nah, D. Yang, R. Piner, A. Velamakanni, I. Jung, E. Tutuc, S.K. Banerjee, L. Colombo, R.S. Ruoff, Large-area synthesis of high-quality and uniform graphene films on copper foils, Science 324 (2009) 1312–1314, https://doi.org/10.1126/science.1171245.

[34] P.Z. Sun, Q. Yang, W.J. Kuang, Y.V. Stebunov, W.Q. Xiong, J. Yu, R.R. Nair, M. I. Katsnelson, S.J. Yuan, I.V. Grigorieva, M. Lozada-Hidalgo, F.C. Wang, A.K. Geim, Limits on gas impermeability of graphene, Nature 579 (2020) 229–232, https://doi.org/10.1038/s41586-020-2070-x.

[35] Y. Tu, J. Deng, C. Ma, L. Yu, X. Bao, D. Deng, Double-layer hybrid chainmail catalyst for high-performance hydrogen evolution, Nano Energy 72 (2020), 104700, https://doi.org/10.1016/j.nanoen.2020.104700.

[36] V. Berry, Impermeability of graphene and its applications, Carbon 62 (2013) 1–10, https://doi.org/10.1016/j.carbon.2013.05.052.

[37] W. Fang, A.L. Hsu, Y. Song, J. Kong, A review of large-area bilayer graphene synthesis by chemical vapor deposition, Nanoscale 7 (2015) 20335–20351, https://doi.org/10.1039/C5NR04756K.

[38] L. Tong, L. Ren, A. Fu, D. Wang, L. Liu, J. Ye, Copper nanoparticles selectively encapsulated in an ultrathin carbon cage loaded on $SrTiO_3$ as stable photocatalysts for visible-light H_2 evolution via water splitting, Chem. Commun. 55 (2019) 12900–12903, https://doi.org/10.1039/c9cc05228c.

[39] L. Ren, L. Tong, X. Yi, W. Zhou, D. Wang, L. Liu, J. Ye, Ultrathin graphene encapsulated Cu nanoparticles: a highly stable and efficient catalyst for photocatalytic H_2 evolution and degradation of isopropanol, Chem. Eng. J. 390 (2020), https://doi.org/10.1016/j.cej.2020.124558.

[40] Q. Yang, H. Liu, P. Yuan, Y. Jia, L. Zhuang, H. Zhang, X. Yan, G. Liu, Y. Zhao, J. Liu, S. Wei, L. Song, Q. Wu, B. Ge, L. Zhang, K. Wang, X. Wang, C.-R. Chang, X. Yao, Single carbon vacancy traps atomic platinum for hydrogen evolution catalysis, J. Am. Chem. Soc. 144 (2022) 2171–2178, https://doi.org/10.1021/jacs.1c10814.

[41] J. Yang, H. Miao, J. Jing, Y. Zhu, W. Choi, Photocatalytic activity enhancement of PDI supermolecular via π-π action and energy level adjusting with graphene quantum dots, Appl. Catal. B Environ. 281 (2021), 119547, https://doi.org/10.1016/j.apcatb.2020.119547.

[42] J.-B. Wu, M.-L. Lin, X. Cong, H.-N. Liu, P.-H. Tan, Raman spectroscopy of graphene-based materials and its applications in related devices, Chem. Soc. Rev. 47 (2018) 1822–1873, https://doi.org/10.1039/C6CS00915H.

[43] X. Jia, J. Campos-Delgado, M. Terrones, V. Meunier, M.S. Dresselhaus, Graphene edges: a review of their fabrication and characterization, Nanoscale 3 (2011) 86–95, https://doi.org/10.1039/C0NR00600A.

[44] L. Zhang, Z. Shi, Y. Wang, R. Yang, D. Shi, G. Zhang, Catalyst-free growth of nanographene films on various substrates, Nano Res. 4 (2011) 315–321, https://doi.org/10.1007/s12274-010-0086-5.

[45] A.T. Garcia-Esparza, T. Shinagawa, S. Ould-Chikh, M. Qureshi, X. Peng, N. Wei, D. H. Anjum, A. Clo, T.-C. Weng, D. Nordlund, D. Sokaras, J. Kubota, K. Domen, K. Takanabe, An oxygen-insensitive hydrogen evolution catalyst coated by a molybdenum-based layer for overall water splitting, Angew. Chem. Int. Ed. 56 (2017) 5780–5784, https://doi.org/10.1002/anie.201701861.

[46] J.A. Bau, K. Takanabe, Ultrathin microporous SiO2 membranes photodeposited on hydrogen evolving catalysts enabling overall water splitting, ACS Catal. 7 (2017) 7931–7940, https://doi.org/10.1021/acscatal.7b03017.

[47] L. Lin, Z. Lin, J. Zhang, X. Cai, W. Lin, Z. Yu, X. Wang, Molecular-level insights on the reactive facet of carbon nitride single crystals photocatalysing overall water splitting, Nat. Catal. 3 (2020) 649–655, https://doi.org/10.1038/s41929-020-0476-3.

[48] G. Zhang, Z.-A. Lan, L. Lin, S. Lin, X. Wang, Overall water splitting by Pt/g-C_3N_4 photocatalysts without using sacrificial agents, Chem. Sci. 7 (2016) 3062–3066, https://doi.org/10.1039/C5SC04572J.

[49] X. Zhang, L. Jian, L. Wang, R. Liu, Y. Zhao, Y. Li, C. Wang, Inhibition of H_2-O_2 recombination using amino functional groups to anchor oxygen for enhancing photocatalytic hydrogen generation, Appl. Surf. Sci. 571 (2022), 151304, https://doi.org/10.1016/j.apsusc.2021.151304.

[50] J. Deng, P. Ren, D. Deng, X. Bao, Enhanced electron penetration through an ultrathin graphene layer for highly efficient catalysis of the hydrogen evolution reaction, Angew. Chem. Int. Ed. 54 (2015) 2100–2104, https://doi.org/10.1002/anie.201409524.

[51] Y. Wang, P. Ren, J. Hu, Y. Tu, Z. Gong, Y. Cui, Y. Zheng, M. Chen, W. Zhang, C. Ma, L. Yu, F. Yang, Y. Wang, X. Bao, D. Deng, Electron penetration triggering interface activity of Pt-graphene for CO oxidation at room temperature, Nat. Commun. 12 (2021) 5814, https://doi.org/10.1038/s41467-021-26089-y.

[52] J.-L. Yang, H.-J. Wang, Z. Zhu, M.-F. Yue, W.-M. Yang, X.-G. Zhang, X. Ruan, Z. Guan, Z.-L. Yang, W. Cai, Y.-F. Wu, F.-R. Fan, J.-C. Dong, H. Zhang, H. Xu, Z.-Q. Tian, J.-F. Li, In situ raman probing of hot-electron transfer at gold–graphene interfaces with atomic layer accuracy, Angew. Chem. Int. Ed. 61 (2022), e202112749, https://doi.org/10.1002/anie.202112749.

[53] M. Qureshi, A.T. Garcia-Esparza, G. Jeantelot, S. Ould-Chikh, A. Aguilar-Tapia, J.-L. Hazemann, J.-M. Basset, D. Loffreda, T. Le Bahers, K. Takanabe, Catalytic consequences of ultrafine Pt clusters supported on $SrTiO_3$ for photocatalytic overall water splitting, J. Catal. 376 (2019) 180–190, https://doi.org/10.1016/j.jcat.2019.06.045.

[54] J. Lian, D. Li, Y. Qi, N. Yang, R. Zhang, T. Xie, N. Guan, L. Li, F. Zhang, Metal-seed assistant photodeposition of platinum over Ta_3N_5 photocatalyst for promoted solar hydrogen production under visible light, J. Energy Chem. 55 (2021) 444–448, https://doi.org/10.1016/j.jechem.2020.07.034.

[55] S. Chen, Z. Wei, X. Qi, L. Dong, Y.-G. Guo, L. Wan, Z. Shao, L. Li, Nanostructured polyaniline-decorated Pt/C@PANI core–shell catalyst with enhanced durability and activity, J. Am. Chem. Soc. 134 (2012) 13252–13255, https://doi.org/10.1021/ja306501x.

[56] W. Zhang, G. Li, W. Wang, Y. Qin, T. An, X. Xiao, W. Choi, Enhanced photocatalytic mechanism of Ag_3PO_4 nano-sheets using MS_2 (M = Mo, W)/rGO hybrids as co-catalysts for 4-nitrophenol degradation in water, Appl. Catal. B Environ. 232 (2018) 11–18, https://doi.org/10.1016/j.apcatb.2018.03.006.

[57] S. Volkening, K. Bedurftig, K. Jacobi, J. Wintterlin, G. Ertl, Dual-path mechanism for catalytic oxidation of hydrogen on platinum surfaces, Phys. Rev. Lett. 83 (1999) 2672–2675, https://doi.org/10.1103/PhysRevLett.83.2672.

[58] A. Michaelides, P. Hu, Catalytic water formation on platinum: a first-principles study, J. Am. Chem. Soc. 123 (2001) 4235–4242, https://doi.org/10.1021/ja003576x.

[59] J. Deng, L. Yu, D. Deng, X. Chen, F. Yang, X. Bao, Highly active reduction of oxygen on a FeCo alloy catalyst encapsulated in pod-like carbon nanotubes with fewer walls, J. Mater. Chem. A 1 (2013) 14868–14873, https://doi.org/10.1039/C3TA13759G.

[60] S. Chen, D. Huang, D. Liu, H. Sun, W. Yan, J. Wang, M. Dong, X. Tong, W. Fan, Hollow and porous $NiCo_2O_4$ nanospheres for enhanced methanol oxidation reaction and oxygen reduction reaction by oxygen vacancies engineering, Appl. Catal. B Environ. 291 (2021), 120065, https://doi.org/10.1016/j.apcatb.2021.120065.

[61] M. Yoshida, K. Takanabe, K. Maeda, A. Ishikawa, J. Kubota, Y. Sakata, Y. Ikezawa, K. Domen, Role and function of noble-metal/Cr-layer core/shell structure cocatalysts for photocatalytic overall water splitting studied by model electrodes, J. Phys. Chem. C. 113 (2009) 10151–10157, https://doi.org/10.1021/jp901418u.

[62] Y. Hang Li, J. Xing, Z. Jia Chen, Z. Li, F. Tian, L. Rong Zheng, H. Feng Wang, P. Hu, H. Jun Zhao, H. Gui Yang, Unidirectional suppression of hydrogen oxidation on oxidized platinum clusters, Nat. Commun. 4 (2013) 2500, https://doi.org/10.1038/ncomms3500.

[63] G. Feng, F. Ning, J. Song, H. Shang, K. Zhang, Z. Ding, P. Gao, W. Chu, D. Xia, Sub-2 nm ultrasmall high-entropy alloy nanoparticles for extremely superior electrocatalytic hydrogen evolution, J. Am. Chem. Soc. 143 (2021) 17117–17127, https://doi.org/10.1021/jacs.1c07643.

[64] T. Xu, D. Jiao, L. Zhang, H. Zhang, L. Zheng, D.J. Singh, J. Zhao, W. Zheng, X. Cui, Br-induced P-poor defective nickel phosphide for highly efficient overall water splitting, Appl. Catal. B Environ. 316 (2022), 121686, https://doi.org/10.1016/j.apcatb.2022.121686.

[65] G. Yao, S. Yang, S. Jiang, C. Sun, S. Song, Spin polarized graphene monolayer of van der Waals heterojunction for photocatalytic H_2O overall splitting, Appl. Catal. B Environ. 315 (2022), 121569, https://doi.org/10.1016/j.apcatb.2022.121569.

[66] Z. Li, L. Zhang, Y. Liu, C. Shao, Y. Gao, F. Fan, J. Wang, J. Li, J. Yan, R. Li, C. Li, Surface-polarity-induced spatial charge separation boosts photocatalytic overall water splitting on GaN nanorod arrays, Angew. Chem. Int. Ed. 59 (2020) 935–942, https://doi.org/10.1002/anie.201912844.

[67] B. Jing, Z. Ao, W. Zhao, Y. Xu, Z. Chen, T. An, Evaluation procedure of photocatalysts for VOCs degradation from the view of density functional theory

calculations: g-C_3N_4 dots/graphene as an, Ex., J. Mater. Chem. A 8 (2020) 20363–20372, https://doi.org/10.1039/D0TA06060G.

[68] S. Dong, Y. Zhao, J. Yang, X. Liu, W. Li, L. Zhang, Y. Wu, J. Sun, J. Feng, Y. Zhu, Visible-light responsive PDI/rGO composite film for the photothermal catalytic degradation of antibiotic wastewater and interfacial water evaporation, Appl. Catal. B Environ. 291 (2021), 120127, https://doi.org/10.1016/j.apcatb.2021.120127.

[69] J. Cui, X. Yang, Z. Yang, Y. Sun, X. Chen, X. Liu, D. Wang, S. Jiang, L. Liu, J. Ye, Zr–Al co-doped $SrTiO_3$ with suppressed charge recombination for efficient photocatalytic overall water splitting, Chem. Commun. 57 (2021) 10640–10643, https://doi.org/10.1039/D1CC04514H.